HHS Public Access

Author manuscript

Microfluid Nanofluidics. Author manuscript; available in PMC 2018 December 12.

Published in final edited form as:

Microfluid Nanofluidics. 2018 March ; 22: .

Normally closed plunger-membrane microvalve self-actuated electrically using a shape memory alloy wire

Chaojun Cheng[1], **Ankitha Rajagopalan Nair**[3], **Raviraj Thakur**[2], and **Gene Fridman**[2,3,4]

[1]Mechanical Engineering, Johns Hopkins University, Baltimore, USA

[2]Otolaryngology HNS, Johns Hopkins University, Baltimore, USA

[3]Biomedical Engineering, Johns Hopkins University, Baltimore, USA

[4]Electrical and Computer Engineering, Johns Hopkins University, Baltimore, USA

Abstract

Various microfluidic architectures designed for in vivo and point-of-care diagnostic applications require larger channels, autonomous actuation, and portability. In this paper, we present a normally closed microvalve design capable of fully autonomous actuation for wide diameter microchannels (tens to hundreds of μm). We fabricated the multilayer plunger-membrane valve architecture using the silicone elastomer, poly-dimethylsiloxane (PDMS) and optimized it to reduce the force required to open the valve. A 50-μm Nitinol (NiTi) shape memory alloy wire is incorporated into the device and can operate the valve when actuated with 100-mA current delivered from a 3-V supply. We characterized the valve for its actuation kinetics using an electrochemical assay and tested its reliability at 1.5-s cycle duration for 1 million cycles during which we observed no operational degradation.

Keywords

Valve; Point-of-care; Nitinol; Self-actuated; PDMS

1 Introduction

The design of microfluidics associated with point-of-care diagnostic applications such as salivary diagnostic platforms requires larger channels that can handle as much as 20 μL of saliva (Herr et al. 2007), autonomous actuation, and portability. Microvalve design and the actuation mechanism are key determinants governing its utility in the resource limited settings. The geometry of the valve should minimize the overall force requirements for the flexible membrane. The valve should be able to control larger channels of 10–100 s of μm in diameter. The actuation mechanism must be on-chip, energy efficient and should easily interface with the valve material. The valve needs to be operated entirely in an autonomous way with the power consumption consistent with the use of a small battery, without the use

Correspondence to: Gene Fridman.

Chaojun Cheng and Ankitha Rajagopalan Nair have contributed equally to this work.

of any external apparatus. The entire assembly should be capable of being packaged in a relatively compact manner while maintaining a robust operation.

Elastomeric plunger-membrane microvalves have been a cornerstone technology for enabling various applications of microfluidic devices in bioanalytical instrumentation (Kim et al. 2012, 2016; Jang et al. 2016; Jensen et al. 2013). These valves are robust in operation, easy to manufacture using standard fabrication techniques (Mohan et al. 2011), and several of them have been integrated in a miniature device for reliable liquid handling strategies (Jensen et al. 2013; Mark et al. 2010). The working principle typically involves deflecting a thin elastic membrane with an attached plunger, often made from poly-dimethylsiloxane (PDMS), to reversibly close/open a fluidic channel in a three-layer device. Out of several actuation mechanisms, pneumatic actuation is the most common. A positive suction is used to deflect the thin elastic membrane to open the valve, whereas pressurized air is used to seal the valve off (Amin et al. 2013; Chuang et al. 2012). Although the device footprint is miniaturized, the method requires off-chip apparatus that typically includes compressed air supply, gas regulators, and a vacuum pump. These valves are useful in applications for which off-chip actuation is available. When on-chip activation is necessary for applications such as some point-of-care technologies and drug delivery systems, this technology is insufficient.

Several microvalves with on-chip autonomous actuation have been reported in the literature (Oh and Ahn 2006; Au et al. 2011). Various phase transformation materials have been suggested for actuating membrane valves, making them suitable for portability. These materials exhibit volumetric changes, which are in turn used to control membrane deflections. They deploy on-board resistive metallic heaters to make them operate autonomously (Augustine et al. 2015). The popular phase change microvalves include the use of wax (Díaz-González et al. 2016), thermoresponsive polymers (pNIPAAM), hydrogels (PEG-diacrylate) (Rogers et al. 2014), alginate, or temperature-sensitive liquid(FC-40) (Augustine et al. 2015). While the fabrication process for these valves is challenging due to the need to integrate these materials inside microchannels, the valves are indeed compact and self-actuated. These valves are characterized by small volume change upon phase transformation and slower response times of tens of seconds to several minutes. Because of these limitations these valves are typically designed to operate for microchannels on the order of tens of microns. Alternative on-board approaches that overcome these challenges consist of piezoelectric (Evans et al. 2010) and electrostatic (Chen et al. 2016) actuation. These are faster, easier to manufacture and can control larger channels, but these mechanisms are typically limited by prohibitively high operational voltages (> 250 V) for their actuation (Desai et al. 2012). Additionally, torque actuated valves (Weibel et al. 2005) have shown autonomous actuation by twisting an embedded screw or a plastic plug (Guler et al. 2017) to close a channel. These single layered valves are simpler in construction compared to three-layer plunger design, but consume more power owing to the high torque and friction considerations.

Shape memory alloy (SMA)-based actuation offers a potential solution in this context owing to its fast response times. Vyawahare et al. (2008) were the first to use a Nitinol shape memory alloy wire for making a PDMS-based microvalve. The Nitinol actuator exhibited a

phase transition upon passing electrical current through it and generated a pull force to open/close the valve. Their device could open and close a 10-μm channel by passing 230-mA current through the shape memory alloy wire. Similarly, Gui and Ren (2011) used a coiled Nitinol wire to build normally open and normally closed microvalves in PDMS. Their design could control a wider microchannel of 60 μm width, but required 1.8 A for its operation. While these reports show preliminary promise of electromechanical-based actuation for making autonomous microvalves, a microvalve design with lower power consumption would make it suitable for portable and field-deployable applications.

In this paper, we use a popular architecture, the plunger-membrane microvalve (Baek et al. 2005), originally designed to be operated pneumatically. Since the valve design requires very low forces to operate, we hypothesized that we could operate similar valves with geometries up to 100 s μm using shape memory alloy activated at ~ 100 mA.

2 Valve design and working principle

We constructed a multilayer plunger-membrane valve actuated electrically using a shape memory alloy. Figure 1a, b shows a schematic representation of the cross-sectional view of the valve. The microvalve consists of three conceptual parts: (1) a thin elastic PDMS membrane with an attached cylindrical plunger, (2) an upper and a lower fluidic channel, and (3) a vertical through hole connecting the two channels. A Nitinol SMA wire was embedded in the membrane layer right above the plunger base.

The SMA wire undergoes a phase transition when an electrical current is passed through it. This results in contraction of its length, thereby generating a pull force on the attached PDMS membrane and subsequently lifting the plunger. The wire relaxes back to its original shape upon withdrawal of the electrical stimulus, allowing the microvalve to close. The driving current and the geometry of the valve determine the amount of force generated and the resulting displacement of the plunger. In our design, the fluidic channels are 1 mm deep and 4 mm wide, while the through hole connecting the top and bottom fluid layer is 0.8 mm in diameter.

3 Methods and materials

3.1 Reagents and materials

Nitinol SMA “muscle” wires of 50 μm diameters, 3–130 MW Flexinol 050 HT, were purchased from Dynalloy, Inc. (Irvine, USA). A two part 184 Sylgard elastomer kit containing poly-dimethylsiloxane (PDMS) pre-polymer mix and a cross-linking agent was purchased from Ellsworth Adhesives (WI, USA). A photocurable polymer resin, B9R- 2, was purchased from B9 Creations (South Dakota, USA). Sodium chloride (NaCl) was purchased from Sigma-Aldrich. Chlorotrimethylsilane was purchased from Sigma-Aldrich and used for surface treatment.

3.2 Device fabrication

The normally closed microvalves are made from PDMS using a soft lithography fabrication protocol. Each valve layer was manufactured separately and assembled. First, CAD designs

were created using the Solidworks software, and molds for each layer were 3D printed (B9Creations, South Dakota) using the photocurable resin. The manufactured valve layers corresponding to the specific three molds are delineated in Fig. 1a. Layer 1 contains the upper channel, the top membrane, and the plunger. Layer 2 contains the through hole and the lower channel. Layer 3 is a non-patterned PDMS base layer.

The printed molds were then rinsed thoroughly in an ultrasound bath with DI water containing a commercial surfactant (dish washing liquid) to remove uncured polymer traces. The molds were then post-cured under UV light for 12 h for further solidity. To peel off the casted PDMS layers easily, the mold surfaces were treated with a corona discharge (BD-20AC, Electro-Technic products) followed by salinization with trimethylchlorosilane. A 10:1 wt% mixture of PDMS pre-polymer and curing agent was degassed in a vacuum chamber to remove any air bubbles and poured over each mold. A 50-μm surgical suture wire loop (approximately 5 mm diameter) was carefully embedded in the uncured polymer in the membrane layer using micromanipulators to position the loop inside the plunger. The assembly was put on a hot plate to cure at a temperature of 90 °C. We intentionally did not embed the Nitinol SMA wire directly in the membrane layer to avoid the thermal damage to the actuator, while PDMS cures. Instead the Nitinol actuator was looped through this suture wire before fixing its ends on a breadboard. All the other layers were then baked in an oven at 90 °C for curing. The PDMS layers were carefully peeled off, then aligned using the alignment marks, and sequentially bonded together using a corona discharge to form the microfluidic valve as shown in Fig. 1c, d. The assembled PDMS chip was mounted on top of a single sided breadboard. The free ends of the embedded Nitinol SMA wire were then anchored to the breadboard nods using a solder (Rosin Core, Alphametals Inc.). It was made sure visually that the wire did not have any sag before anchoring it to the breadboard.

3.3 Electrochemical assessment of valve opening and closure

We used an electrochemical assay to study microvalve performance, similar to a previously described study (Chen et al. 2008). This electrochemical assay compared to a flow-based assay offers higher-precision monitoring of valve leaks. To assess the valve performance during its operation, we applied an AC signal across the fluidic channel containing an electrolyte solution as shown in Fig. 2. In the closed state (Fig. 2a), available cross-sectional area at the valve seat for ionic transport is minimized, resulting in larger impedances when compared to an open valve (Fig. 2b). We can differentiate between the different valve states: open, closed, and partially open/closed by comparing the strength of ionic currents flowing through the channel. After the valve fabrication step, the channels were filled with an aqueous electrolyte, containing 1-M sodium chloride dissolved in deionized (DI) water. We made sure that there were no air bubbles in this pre-filling step, as they significantly alter the electrical resistances, thereby impacting the results. Two copper electrodes were inserted upstream and downstream of the valve in the upper and lower fluidic channels, respectively. The electrodes were connected to a function generator, which provides an input signal of 5 V at 1 kHz across the embedded electrodes. The current was measured from the voltage measured across a 56-Ωm sense resistor using an oscilloscope. The electrical test circuit used is shown in Fig. 2a. The input signal frequency of 1 kHz was chosen to minimize the damage to the electrodes during the measurements. Such electrode damage occurs at lower

frequencies owing to the irreversible Faradaic reactions. The kinetics of valve operations including valve opening times, closing times, and percentage of valve opening were determined by observing the temporal changes to the output signal as a function of several actuation parameters. We defined the open state of the valve to be indicated by an impedance of under 2 KΩ and the closed state to be indicated by 20 KΩ or above (10× the open state impedance). Based on the calculation of charge per unit time at 5 V, the number of sodium ions that flow through the valve is 2.7 nmol/s in closed state.

3.4 Effect of plunger radius and height

The required pull force necessary to open the valve must be minimized to lower the power consumption. Even though there are several parameters in the valve design that affect the pull force, we identified the plunger diameter and height as the key parameters that dictate the bending characteristics of the flexible membrane. A thinner membrane requires less pull force to open the valve fully, but owing to our large channel width, the thin membrane can potentially sag into the channels. Membrane sagging can lead to a pre-stressed membrane valve, heavily influencing the valve performance. Thus, the membrane thickness was kept constant at 100 μm for this study. We did not observe any visual sagging of the membrane at this thickness.

We fabricated three valves of each different plunger height to study their effect on the required pull force. We designed valves with plunger heights of 0.9, 0.95, 1, and 1.05 mm keeping the plunger radius constant at 1.2 mm (12 valves total). Similarly, to test the effect of plunger radius, we fabricated three valves each with radii 1.2, 1.4, 1.6, and 1.8 mm, while keeping the plunger height constant at 0.95 mm (12 valves total).

The valve opening and closing were assessed using the electrochemical circuit. The two free ends of the SMA wire were attached to a micromanipulator and displaced to mimic the shape memory alloy actuation. The resulting pull force on the wire was recorded using a force gauge, while observing the valve states electrochemically.

3.5 Effect of driving current amplitude and its frequency

We studied the effect of the driving current signal on the valve performance. In this case, a function generator was attached to the soldered ends of the Nitinol SMA wire to vary the driving current signal’s amplitude and frequency. The resulting effect on the valve performance was reflected in the measured electrochemical current. The amplitude of the driving current determines the contraction length of the Nitinol wire and significantly affects the generated pull force. We varied the current amplitudes from 0 to 150 mA keeping the frequency fixed at 0.67 Hz (1.5 s period). The voltage across the SMA wire ranged between 0 and 3 V for this experiment. For evaluating the response time of the valve, we varied the frequency of the actuation pulse, while keeping its amplitude fixed at 95 mA.

3.6 Valve leakage test

We performed a leakage test of the microvalve to determine the threshold pressure beyond which the valve leaks substantially. Owing to its geometrical asymmetry, we tested the valves in both directions to determine the forward and the backward leakage pressure. In the

"forward" direction, we pressurized the inlet (layer 1) using fluid pressure upstream of the valve, while maintaining the atmospheric pressure downstream at the outlet (layer 2). Analogously, in the "backward" direction the outlet was pressurized relative to the valve inlet which was kept at atmospheric pressure. The leakage was determined by measuring the change in the electrical impedance across the microvalve, and corresponding pressure was monitored by a pressure gauge.

3.7 Long-term reliability test

The microvalve design was subjected to long-term reliability test to identify failure mechanisms. We recognized two possible scenarios of valve failure. One is the fatigue failure of the actuator SMA wire itself owing to irreversible changes upon long-term electrical actuation. In this case, the wire can become permanently elongated or break. The second possible failure point is the joint between the SMA wire and the PDMS membrane at the embedding junction. We performed two tests where the Nitinol wire was actuated with a driving current of 105 mA ($N = 2$) and 160 mA ($N = 1$), respectively, while keeping the cycle duration at 1.5 s. Its performance was recorded at intermediate time points using the electrochemical impedance assay as described earlier. It is known that higher current can accelerate the fatigue failure process, owing to an increased heating of the shape memory alloy. Thus, the valve test with 160-mA actuation current also served as our negative control to validate the assay. Electrode degradation and electrolyte evaporation posed a challenge in this experiment. To overcome this issue, we inserted new electrodes and a freshly made electrolyte at each time point during the measurements.

4 Results and discussion

4.1 Effect of plunger radius and height

The effect of plunger size on the required pull force is summarized in Fig. 2c, d. The electrochemical impedance assay was used to assess the valve opening and closure. The measured open valve impedance of each variant was found to decrease by two orders of magnitude as the valve changed its state from closed to open upon the application of force. Figure 2c indicates that the pull force needed to open the valve decreases with the decreased plunger height. For a plunger with a height of 1.05 mm, the required pull force for a complete valve opening was found to be around 20 g, whereas for the plunger height of 0.9 mm, the force was around 7.5 g. This trend can be explained by considering that the opening covered by the plunger was slightly elevated during the manufacturing process due to surface tension. During curing, this surface tension created a meniscus at the part of the mold filling the opening. The result was that the higher height plungers created a stress on the top membrane that was greater than that due to the smaller height plungers in their resting state. This tension therefore required a larger force to lift the higher height plungers. At 0.9 mm plunger height, the impedance when no pull force was applied was very near the limit for closed state impedance (20 KΩ), whereas for the higher height plungers, this closed state impedance was reached at higher forces. We accepted this plunger height as the lower limit for this parameter because decreasing the plunger height beyond this point may not be desired owing to the increase in the closed state leakage currents.

The effect of the plunger radius on the valve performance is plotted in Fig. 2d. The required pull force increased with the radius of the plunger. At 1.2 mm, the force required to fully open the valve was found to be around 10 g, whereas for the radius of 1.8 mm, it was around 20 g. This direct relationship between the plunger radius and the force necessary to open the valve could be due to the added contact area around the valve opening, resulting in surface area tension due to stiction. Based on these characterizations, we concluded that the height of 0.95 mm and radius of 1.2 mm were optimum parameters (i.e., requiring minimum force, while being able to fully open and close) for our subsequent electrical tests.

4.2 Measurement of valve opening and closing times

The opening and closing kinetics of the optimized microvalve design are shown in Fig. 3a. The plot shows the time course of measured electrochemical current flowing through the valve as a function of the applied electrical stimulus in the Nitinol actuator. A time delay of $\tau_{onset} = 0.265$ s was observed from the point of the application of the trigger to the point where the valve starts to respond. This observed time lag is composed of two components. When an electrical current is passed through the actuator, there is an intrinsic time delay associated with the phase transition within the shape memory alloy. Secondly, there is a bonding force (stiction) initially present between the plunger base and the channel. If the applied force on the membrane is not greater than this bonding force, the valve remains in a closed state. However, as soon as the pull force is greater than this threshold value, the membrane is lifted from the surface and the reactionary force component disappears leading to a rapid membrane motion in response to the electrical trigger. This membrane motion is reflected in the rise of the electrochemical current as seen in the plot. For the valve tested, the time constant for this process was found to be $\tau_{rise} = 0.07$ s. For the applied pulse width of 0.75 s, the valve remained in the fully open state for $\tau_{dwell} = 0.265$ s. As the electrical pulse was withdrawn after 0.75 s, the measured electrochemical current diminished to its baseline value reflecting the closed valve state. The relaxation time of $\tau_{offset} = 0.09$ s was observed from the withdrawal of the current from the wire to when the valve responded to this change. This time lag represents the time associated with the cooling of Nitinol muscle wire to the temperature below its phase transition of ~ 78 °C. Once the muscle wire is sufficiently relaxed the time constant for closing the valve due to its elasticity was found to be $\tau_{fall} = 0.02$ s.

4.3 Effect of driving current amplitude and its frequency

Figure 3b shows the effect of driving current amplitude on the valve performance. The plot indicates that the current driving the SMA wire needs to be greater than 95 mA to open the valve. The transition between open and closed states is rather sudden, occurring within only 10 mA between 90 and 100 mA. We attribute this sudden transition to the bonding force between the plunger base and channel surface as explained in the earlier section. Figure 3c shows the variation of open valve impedances as a function of frequency, while maintaining the optimized current amplitude of 95 mA flowing through the SMA actuator. The valve remained in the closed state for frequencies higher than 4 Hz. For the driving frequencies in the range of 2–4 Hz, the valve opened partially. And for frequencies lower than 2 Hz, the valve could fully open. This observed frequency behavior can be explained by considering onset time lags as discussed in the previous section. The amount of contraction and the

resulting force in Nitinol actuator strongly depend on the pulse duration. At higher frequencies, there is not enough time for the shape memory alloy to fully contract, resulting in the valve maintaining its idle closed state. At low frequencies, the actuator has enough time to contract fully, thereby opening the valve completely. At the intermediate frequencies, the actuator contracts only partially, subsequently making the valve partially open.

4.4 Long-term reliability test

Figure 4 shows the variation of normalized current flowing through the valve in its open state as a function of the number of actuation cycles. For the optimized driving current of 105 mA through the actuator wire, there was no appreciable change in normalized current for one million cycles. In contrast, when the valve was driven at 160 mA, there was a significant decrease in the open valve current only after 3600 cycles, indicating that the valve did not open afterward when actuated. We inspected the failed microvalve to identify possible sources of failure and confirmed that the joint between the wire and the PDMS membrane was intact. However, the Nitinol SMA wire itself was found broken as the result of the higher driving current, in turn failing the valve actuation. We conclude that the longevity of the valve is a strong function of the driving current and that the test and the assay are sensitive enough to detect valve failure. For optimal operation, the microvalve design appears to reliably operate for one million cycles, when operated at driving currents of 105 mA.

4.5 Valve leakage test

The electrochemical current measured when the valve is closed represents the leakage value in our experiments with zero back pressure and was found to be substantially lower than when the valve is open. How a positive and negative back pressure affects the overall valve leakage is important for applications which involve fluids under flowing conditions. The pressure–impedance plots are summarized in Fig. 5. As the applied pressure increased from either the inlet or the outlet, the valve impedance decreased indicating the valve leakage. We observed that a threshold pressure of 1 psi forced the valve open from the normally closed position in the forward direction (when the pressure was applied at the inlet), whereas that threshold pressure in the backward direction (when the pressure was applied at the outlet) was found to be 3 psi.

5 Conclusion

We presented a microfluidic design for a self-actuated SMA wire actuated valve. The valve is designed for larger caliber microfluidic channels ranging from 10 to 100 s of μm in diameter. The valve can be operated at up to 2 Hz at 95-mA activation current. The time to open the valve is ~ 0.5 s, and it takes ~ 0.25 s to close the valve. The valve is designed for a switch type of operation rather than a gradual flow control. We confirmed the reliable operation of the valve for 1 million cycles.

The microvalve was manufactured using standard microfabrication steps in PDMS and thus can be integrated with other microfluidic systems employing these materials and manufacturing techniques. We believe this efficient self-actuated valve mechanism will be

useful for the portable microfluidic devices especially in the field of in vivo drug delivery and point-of-care diagnostics.

Acknowledgments

We thank Kevin King, Annie Mao, and Scott Sterrett for previous microfluidics work toward safe DC stimulator design. We also acknowledge the funding sources that made this work possible: MedEl Corporate Grant: FK2350 and NIH R01NS092726.

References

Amin AM, Thakur R, Madren S. , et al. Software-programmable continuous-flow multi-purpose lab-on-a-chip. Microfluid Nanofluidics. 2013. https://doi.org/10.1007/s10404-013-1180-2

Au AK, Lai H, Utela BR, Folch A. Microvalves and micropumps for BioMEMS. Micromachines. 2011; 2:179–220.https://doi.org/10.3390/mi2020179

Augustine S, Gu P, Zheng X, et al. Low-power electrically controlled thermoelastic microvalves integrated in thermoplastic microfluidic devices. Microfluid Nanofluidics. 2015; 19:1385–1394.https://doi.org/10.1007/s10404-015-1653-6

Baek JY, Park JY, Ju JIl, et al. A pneumatically controllable flexible and polymeric microfluidic valve fabricated via in situ development. J Micromechanics Microengineering. 2005; 15:1015–1020.https://doi.org/10.1088/0960-1317/15/5/017

Chen H, Gu W, Cellar N, et al. Electromechanical properties of pressure-actuated poly (dimethylsiloxane) microfluidic push-down valves. Anal Chem. 2008; 80:6110–6113. [PubMed: 18576665]

Chen S, Lu S, Liu Y. , et al. A normally-closed piezoelectric micro-valve with flexible stopper. AIP Adv. 2016. https://doi.org/10.1063/1.4947301

Chuang H-S, Thakur R, Wereley ST. Characterizations of gas purge valves for liquid alignment and gas removal in a microfluidic chip. J Micromechanics Microengineering. 2012. https://doi.org/10.1088/0960-1317/22/8/085023

Desai AV, Tice JD, Apblett CA, Kenis PJA. Design considerations for electrostatic microvalves with applications in poly(dimethylsiloxane)-based microfluidics. Lab Chip. 2012; 12:1078.https://doi.org/10.1039/c2lc21133e [PubMed: 22301791]

Díaz-González M, Fernández-Sánchez C, Baldi A. Multiple actuation microvalves in wax microfluidics. Lab Chip. 2016. https://doi.org/10.1039/C6LC00800C

Evans AT, Park JM, Chiravuri S, Gianchandani YB. A low power, microvalve regulated architecture for drug delivery systems. Biomed Microdevices. 2010; 12:159–168.https://doi.org/10.1007/s10544-009-9372-y [PubMed: 19936930]

Gui L, Ren CL. Exploration and evaluation of embedded shape memory alloy (SMA) microvalves for high aspect ratio microchannels. Sensors Actuators A Phys. 2011; 168:155–161.https://doi.org/10.1016/j.sna.2011.03.038

Guler MT, Beyazkilic P, Elbuken C. A versatile plug microvalve for microfluidic applications. Sensors Actuators A Phys. 2017; 265:224–230.https://doi.org/10.1016/j.sna.2017.09.001

Herr AE, Hatch AV, Throckmorton DJ, et al. Microfluidic immunoassays as rapid saliva-based clinical diagnostics. Proc Natl Acad Sci. 2007; 104:5268–5273.https://doi.org/10.1073/pnas.0607254104 [PubMed: 17374724]

Jang L-W, Razu ME, Jensen EC, et al. A fully automated microfluidic micellar electrokinetic chromatography analyzer for organic compound detection. Lab Chip. 2016; 16:3558–3564.https://doi.org/10.1039/C6LC00790B [PubMed: 27507322]

Jensen EC, Stockton AM, Chiesl TN, et al. Digitally programmable microfluidic automaton for multiscale combinatorial mixing and sample processing. Lab Chip. 2013; 13:288–296.https://doi.org/10.1039/C2LC40861A [PubMed: 23172232]

Kim J, Kang M, Jensen EC, Mathies RA. Lifting gate polydimethylsiloxane microvalves and pumps for microfluidic control. Anal Chem. 2012; 84:2067–2071.https://doi.org/10.1021/ac202934x [PubMed: 22257104]

Kim J, Stockton AM, Jensen EC, Mathies RA. Pneumatically actuated microvalve circuits for programmable automation of chemical and biochemical analysis. Lab Chip. 2016; 16:812–819.https://doi.org/10.1039/C5LC01397F [PubMed: 26864083]

Mark D, Haeberle S, Roth G. , et al. Microfluidic lab-on-a-chip platforms: requirements, characteristics and applications. NATO Sci Peace Secur Ser A Chem Biol. 2010. https://doi.org/10.1007/978-90-481-9029-4-17

Mohan R, Schudel BR, Desai AV, et al. Design considerations for elastomeric normally closed microfluidic valves. Sensors Actuators B Chem. 2011; 160:1216–1223.https://doi.org/10.1016/j.snb.2011.09.051

Oh KW, Ahn CH. A review of microvalves. J Micromechanics Microengineering. 2006; 16:R13–R39.https://doi.org/10.1088/0960-1317/16/5/R01

Rogers CI, Oxborrow JB, Anderson RR, et al. Microfluidic valves made from polymerized polyethylene glycol diacrylate. Sensors Actuators B Chem. 2014; 191:438–444.https://doi.org/10.1016/j.snb.2013.10.008

Vyawahare S, Sitaula S, Martin S, et al. Electronic control of elastomeric microfluidic circuits with shape memory actuators. Lab Chip. 2008; 8:1530.https://doi.org/10.1039/b804515a [PubMed: 18818809]

Weibel DB, Kruithof M, Potenta S, et al. Torque-actuated valves for microfluidics. Anal Chem. 2005; 77:4726–4733.https://doi.org/10.1021/ac048303p [PubMed: 16053282]

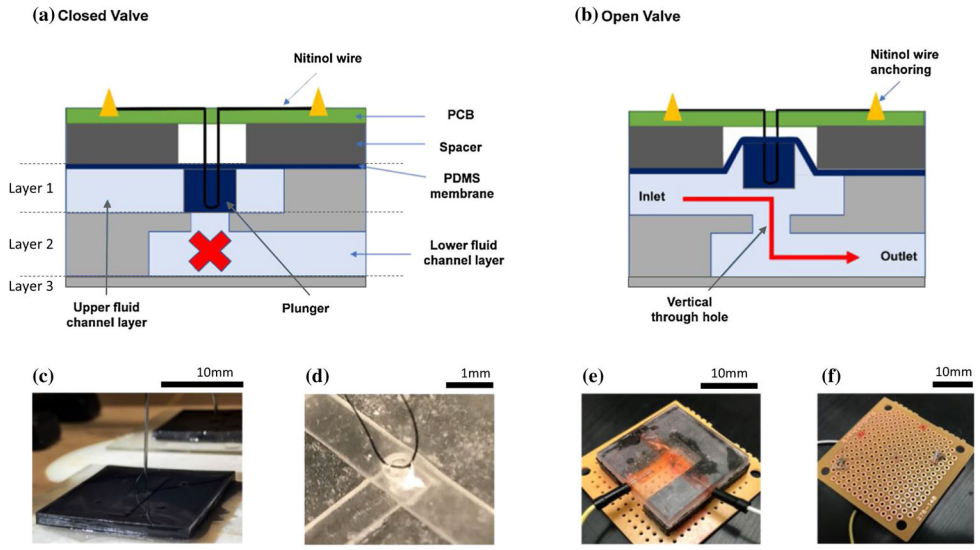

Fig. 1.

Microvalve design and fabrication. **a** Schematic representation of the microvalve cross section. Under no electrical actuation, the valve is in closed state. The layers 1, 2, 3 delineate the parts of the valve that were manufactured from the same molds. **b** When the Nitinol wire is actuated electrically, pull force generated on the membrane lifts the plunger upward thereby opening the valve. **c** Image shows the process of embedding 50-μm surgical suture wire in the uncured polymer matrix. The Nitinol SMA wire was looped around this suture in the final assembly. **d** Image showing the embedded surgical suture wire in the PDMS membrane layer after the polymer has cured. **e** The assembled microvalve with copper electrodes embedded in the inlet and the outlet for electrochemical impedance testing. **f** Nitinol wire anchoring for electrical actuation using low temperature solder

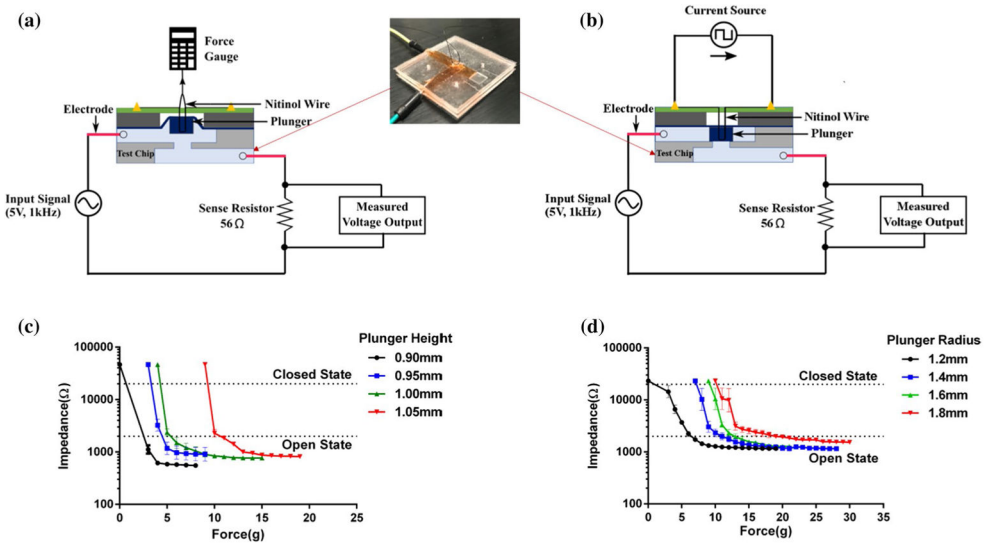

Fig. 2.

a Schematic for the characterization setup and electrical test circuit for optimizing pull force for the plunger-membrane microvalve. Inset image shows valve carrying a 1-M NaCl electrolyte solution in the channels along with two copper electrodes for electrochemical assy. **b** Test setup showing the electrical actuation of Nitinol SMA wire using a pulse generator. **c** Force–impedance characteristic plot for plungers of different heights. **d** Force–impedance characteristics plot for plungers of different radii. $N = 3$ chips tested for each plunger height in **b** and each plunger radius in **c**. Error bars represent standard deviation of the measurements

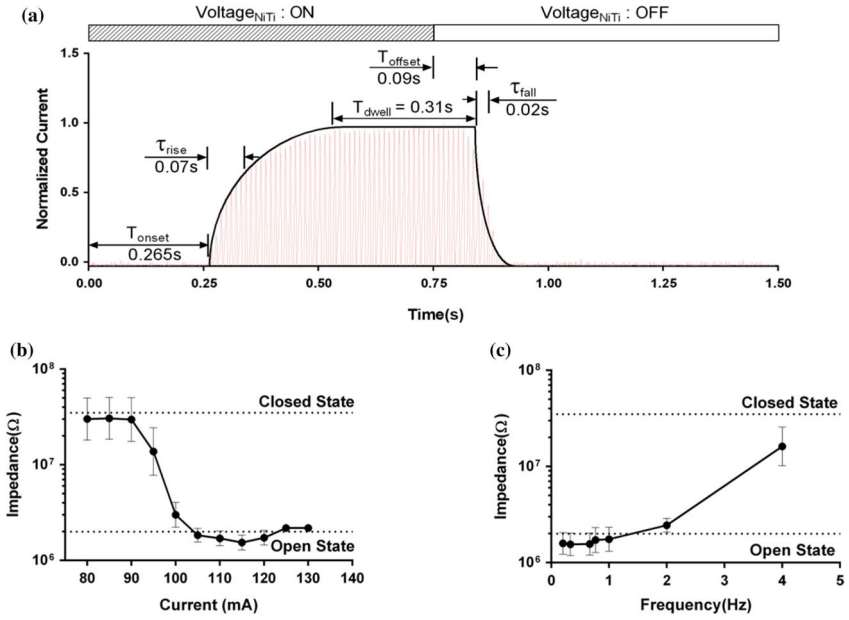

Fig. 3.

Electrical actuation of the plunger-membrane microvalve. **a** A current response of the microvalve for Nitinol actuation current of 100 mA for a driving current pulse width of 0.75 s at 95 mA followed by a relaxation time of 0.75 s at zero current. **b** The valve impedance as a function of amplitude of driving current flowing through the actuator. **c** The minimum valve impedance as a function of frequency of the applied pulsed signal passing through the actuator. We identity a closed valve when the measured impedance values are at least an order of magnitude higher than impedance values for the open valve. The error bars represent standard error mean for $N = 3$ chips tested

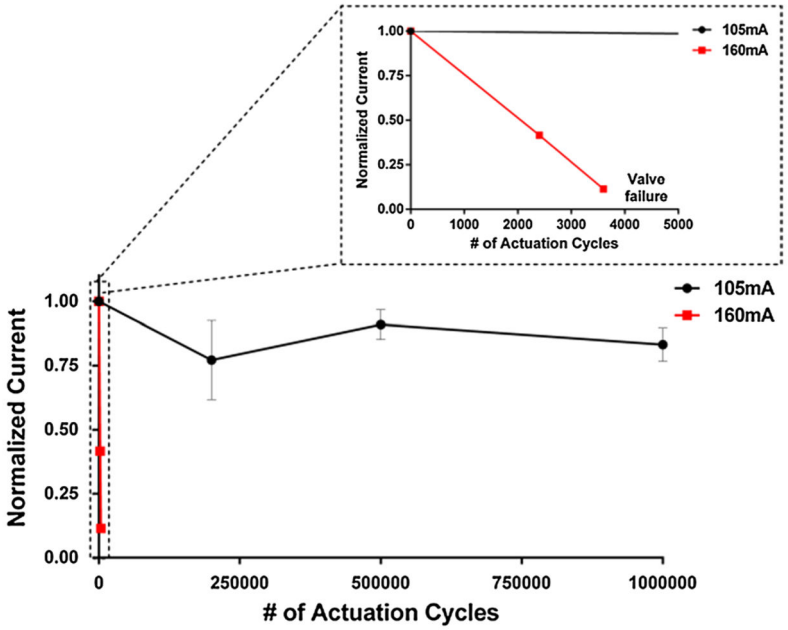

Fig. 4.

Plot showing long-term testing of the plunger-membrane microvalve at 105 and 160 mA driving current. The open valve electrochemical current is shown on the *y*-axis, normalized to the starting current. $N = 2$ for 105 mA test and $N = 1$ for the 160 mA control

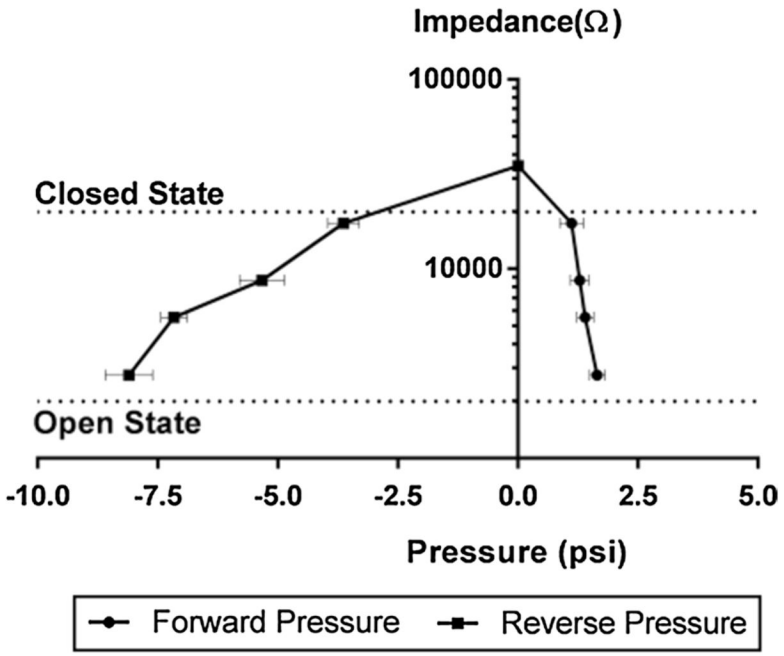

Fig. 5.

Plot showing pressure–impedance characteristics of the plunger-membrane microvalve during the leakage test. The valve impedance decreases with increasing inlet (positive or "forward") pressure or with increasing outlet (negative or "reverse") pressure reflecting the leakage incurred. The data were obtained for $N = 3$